IEEE Access
Multidisciplinary ⋮ Rapid Review ⋮ Open Access Journal

Received January 11, 2022, accepted February 11, 2022, date of publication February 24, 2022, date of current version March 7, 2022.

Digital Object Identifier 10.1109/ACCESS.2022.3154058

A Method for Real-Time Prediction of the Probability of Voltage Sag Duration Based on Harmonic Footprint

ALEKSANDAR M. STANISAVLJEVIĆ, (Member, IEEE), VLADIMIR A. KATIĆ, (Senior Member, IEEE), AND SRĐAN LJ. MILIĆEVIĆ
Faculty of Technical Sciences, University of Novi Sad, 21000 Novi Sad, Serbia

Corresponding author: Vladimir A. Katić (katav@uns.ac.rs)

This work was supported by the Republic of Serbia, Ministry of Education, Science, and Technological Development, through the Integrated and Interdisciplinary Research project entitled "Innovative Scientific and Artistic Research from the Faculty of Technical Sciences Activity Domain" under Grant No. 451-03-68/2022-14/200156.

ABSTRACT In this paper, a novel method for real-time prediction of voltage sag duration is proposed. It is based on the recently introduced new characteristic of voltage sag, named harmonic footprint, and is formulated using a logistic regression model. The concept is mathematically formulated and statistically analyzed using an extensive set of real grid measurement data which are recorded in distribution grids. Furthermore, the proposed method is applied as a part of an advanced grid-tie converter control. It is included in previously developed methods for fast sag detection and magnitude of voltage sag prediction. The algorithm is applied to the control of grid-tie converters used in distributed generators and tested with real/grid measurement data in the IEEE 13-bus test grid by simulations and in the IEEE 33-bus test grid using a hardware-in-the-loop (HIL) microgrid laboratory testbed. It is shown that this method can prevent unnecessary tripping of distributed generators (DG) and improve low-voltage ride-through (LVRT) support. In addition, the model has the potential to be applied to a wide range of devices or algorithms for the protection, monitoring, and control systems of distribution grids.

INDEX TERMS Power quality, signal analysis, power system faults, inverters, digital control.

I. INTRODUCTION

Modern distribution networks are characterized by increased penetration of distributed energy resources (DERs), that is, distributed generators (DGs) based mainly on renewable energy sources (RESs). The Distribution System Operator (DSO) or Distribution Network Operator (DNO) has a major role in managing energy from the generation sources to the consumers, in ensuring reliability and efficiency in the operation of systems that have DERs, and in providing the quality of supply (specified electric energy quality or power quality (PQ) parameters and quality standards) for servicing system users [1].

Voltage sags or dips are among the most important PQ parameters in contemporary distribution grids. They are a consequence of faults in the power grid, high-power induction motors starting, utility transformer energizing, etc. Their effects can be observed over a wide area, affecting a large number of loads and connected distributed energy resources [2], [3]. Voltage sags are represented by a momentary decrease (10% to 90%) in root-mean-square (RMS) value of the AC voltage (at one, two, or all lines) at the power frequency of duration of 0.5 cycles to 1 min [4], or defined as a sudden reduction in the voltage at a point in the electrical system, with a duration between half a cycle to a few seconds [5]. Negative effects are well-known and may be followed by significant financial losses [6], [7]. They range from a disturbance in the supply of PCs or similar low-power electronic devices to problems in the operation of computers or data centers, industrial drive tripping, or discontinuation of DER generation. Hence, they can both be seen on the demand and generation sides.

On the demand side, to sustain operation and prevent load tripping-off, voltage-tolerant or ride-through curves

The associate editor coordinating the review of this manuscript and approving it for publication was Arash Asrari.

were set for computer (microprocessor-based) equipment by ITIC/CBEMA [8], [9]. However, fulfilling these requirements is insufficient to prevent negative effects. To mitigate them, different types of low-power uninterruptible power supplies (UPSs) [10], or utilization of PQ conditioning devices, such as Ferroresonant transformers [11], Dynamic Voltage Restorers (DVRs) [12], Unified Power Quality Conditioners (UPQCs) [13], Universal Power Quality Conditioning Systems (UPQCSs) [14], distribution static compensators (DSTATCOM) [15], or others have been proposed. It is important to emphasize that for their proper operation voltage sag detection, voltage reference generation (synchronization) and adequate control are essential [16]. Different methods have been proposed for the aforementioned devices [16], [17]. However, there is room for improvement, especially regarding the detection speed, full characterization, and control robustness.

The DNO role is connected to energy management, that is, proper operation of the generation side and energy transfer to the users, so different strategies are used (centralized, decentralized, decentralized multi-agent-based, etc.), especially in the case of faults [18], [19]. If there are instantaneous, momentary, or temporary PQ problems (such as voltage sags), the DNO should react promptly, as it will affect the generation ability of the DER. Besides protection of DERs (voltage sags may provoke current overload, control circuit miss operation due to loss of synchronization, an increase in DC link voltage, DC power oscillation, decrease in the lifetime of power switching devices and DC link capacitors, etc. [20], [21]), the DNO may have some specific or even opposite requirements for operation of DERs during a fault. They are given in national grid code rules and respective standards to enable low-voltage ride-through (LVRT). They are stipulating that a DER should stay connected during a voltage sag for a predefined short time and support the grid by providing a certain amount of reactive power (Q) and active power (P) depending on the voltage sag depth and duration [22], [23]. This task requires momentary adaptation of the DER control system and the setting of a new operation point [24]–[27]. As swift voltage sag detection and characterization are required, improvements to existing methods are needed, again.

Voltage sags are commonly characterized by magnitude and duration which can be easily extracted from standard RMS measurements [28]. Other interesting features include imbalance, phase-angle jump, etc [3]. For the interconnection of modern DERs to the grid, detection of voltage sags is vital, as is the determination of their magnitude (the lowest voltage in all phases), unbalance, and duration (the longest duration measured across all channels) [24], [25].

There are different methods for obtaining these characteristics: conventional methods [4], [5], [28], event estimation-based [29], [30], signal processing [31]–[34], advanced transformation methods [35]–[39], and methods with additional processing, including advanced neural networks (machine learning and artificial intelligence) [29], [32], [40]–[46].

In previous studies, the authors introduced a harmonic footprint method for voltage sag characterization. It demonstrated superior performance for voltage sag detection, magnitude prediction, and imbalance [40], [47]. It was shown, that the voltage sag detection time could be shortened to less than 1 ms [40]. Further research revealed that additional acceleration can be achieved if the harmonic footprint is used for the magnitude of the voltage sag (MoVS) prediction. It was shown that MoVS can be predicted with 95% accuracy and an average time gain for the early determination of 292 ms [47]. However, the voltage sag duration was not treated.

The voltage sag duration depends on the fault-clearing time provided by electrical protection in the power system (current-limiting fuses, expulsion fuses, distance relays, differential relays, overcurrent relays, etc.) or on the acceleration time of a large AC load or transformer energizing time. Usually, the fault clearing time is in the span of 10 ms to 2 s [48], so sag duration ranges from half a cycle to 1 minute [4], [5]. However, in practical meshed networks with differently tuned protective relays, in cases of application of fuse saving strategy and in grids where there are several connected DERs, the duration of the voltage sag at a DER interconnection bus may not be straightforward. Therefore, introducing a method for predicting voltage sag duration may be useful.

In this paper, the authors present a probabilistic method for the real-time prediction of voltage sag duration based on the harmonic footprint. The main idea is to improve the DER operation by anticipating the sag duration during the transient stage of a fault. The harmonic footprint (selected set of harmonics) was used as the main sag feature to achieve this solution. To the best of our knowledge, no real-time method has yet been published. The establishing of the mathematical model and verification using a set of voltage sags data obtained by real-grid measurements are presented. Such a solution is implemented for DER control circuit improvement and tested in a modified IEEE 13-bus test grid. Further validation was performed using a hardware-in-the-loop (HIL) microgrid system with the IEEE 33-bus test grid, where the method was implemented in a wind turbine grid-tied inverter. It is shown, that the method can prevent unnecessary tripping of DERs and improve LVRT support. However, there are other possible applications such as in the control units of DVRs, UPQCs, UPQCSs, DSTATCOMs, etc., but they will be addressed in future work.

The main contributions of this paper are as follows:

- A method for the real-time prediction of probability (RTPP) of voltage sag duration based on harmonic footprint has been proposed;
- The proposed method was verified by testing using real grid measurement data;
- It was applied in a DER control unit;
- The usefulness of the proposed method was tested using simulations and a laboratory Microgrid HIL testbed on

IEEE 13-bus and IEEE 33-bus test grids, respectively, and
- A comparison of a DER operation with and without proposed method implementation was performed and benefits are noted.

The paper is organized as follows: the background and literature overview are presented in Section II. The proposed method for RTPP of voltage sag duration, with mathematical analysis, examination of model effectiveness, and discussion are given in Section III. The RTTP algorithm with model implementation, including early detection and magnitude of voltage sag prediction, is described in Section IV. Applications of the proposed method for the grid-tied inverter operation, and application in the IEEE 33-bus Microgrid HIL setup, and for protection circuit are presented in Section V. Testing of the proposed method using real-grid measurement results by the MATLAB/Simulink model of the IEEE 13-bus test grid and using an advanced Microgrid HIL-based real-time laboratory testbed with an implemented IEEE 33-bus test grid, as well as a discussion of the presented results, are presented in Section VI. The rest of the paper is composed of conclusions, acknowledgments, and references.

II. BACKGROUND AND LITERATURE OVERVIEW

A. VOLTAGE SAGS DURATION CLASSIFICATION IN STANDARDS

Classification of voltage sags according to the magnitude-duration plane, as recommended by IEEE 1159 [4], divides sags into three groups: instantaneous with a duration between 8.3 ms and 0.5 s (or 10 ms and 0.6 s in case of 50 Hz AC networks), momentary with a duration between 0.5 s and 3 s (or 0.6 s and 3 s in case of 50 Hz AC networks) and temporary sags with a duration between 3 s and 60 s.

If LVRT requirements are considered, the sag is either instantaneous/momentary or temporary. According to IEEE Std. 1547-2018 [23], and following LVRT recommendations (grid codes) [22], a protective device will trip only if the sag is deep (less than 55% of rated voltage and with a duration of above 160 ms). In other cases, it may ride through or trip, or it has permissive or mandatory operation capability. Therefore, there may be two possible states: stay connected (in cases of instantaneous/momentary sags of duration less than 3 s), or disconnection is allowed (in cases of temporary sags of duration above 3 s). Similar actions should be taken if the German grid code or some other grid code is applied, i.e., if a sag falls above or below the LVRT line. After 3 s, the DG is not obligated to stay connected to the grid, regardless of the MoVS, both in the IEEE recommendations and in the grid code requirements. In addition, because of the high stress on the inverter components, disconnection is likely justified after 3 s, even if LVRT may continue.

B. HARMONIC FOOTPRINT

The novel real-time method proposed in this study is based on the harmonic footprint (HF), a recently introduced voltage sag indicator [40]. The HF is a voltage sag pattern obtained by tracking the voltage harmonic distortion represented by the sum of the 2^{nd}, the 3^{rd}, the 5^{th}, and the 7^{th} harmonics (HDU2357) during the transition phase of the voltage sag. It usually appears twice during a fault: at the beginning (starting) phase and at the end of the recovery phase of the sag.

The HF has four main characteristics: 1) initialization or starting phase (exponential rise) suitable for detection, 2) maximum value (MHDU), 3) width, and 4) duration. They carry information about the voltage sag's beginning (starting) and magnitude, whereas its duration can be predicted as the probability of developing into a momentary or temporary one, which will be presented further in this paper.

C. LITERATURE OVERVIEW OF VOLTAGE SAGS PREDICTION METHODS

Usually, the determination of the duration of voltage sags is a part of the methods developed for voltage sag prediction. These methods predict the frequency of a voltage sag occurrence during a given time interval and its typical characteristics (magnitude and duration). Computer simulations and long-term measurement data analyses were performed.

Stochastic assessment is the most frequently applied in simulations and includes the critical distance, fault positions, and Monte Carlo (MC) methods. It combines deterministic results with stochastic data to produce a probabilistic assessment of the voltage sags at a given bus in a system [49]–[53]. In [49], a short overview of prediction methods, from essential ones (voltage divider and critical distance) to advanced stochastic methods, is presented. Detailed stochastic models are required to achieve good results and to consider the second-order events. In [50], it was concluded that the method of the critical distances yields acceptable results and is far more accurate than the method of fault positions, but it requires high computational effort. In [51], a state-of-the-art offline method based on the stochastic prediction of the duration and magnitude of the voltage sag was presented. The results show a higher accuracy of the presented method in comparison to the traditional techniques. However, this method is considerably more complex. In [52], the application of stochastic-based methods for network planning was addressed. It successfully predicts proper fault parameters, whereas the entire method for grid planning shows ''adequate'' results. MC simulations were used to predict the voltage sags [53]. It is shown that the MC simulation provides a more comprehensive characterization than the fault position (location) method.

Another approach is to use the recorded voltage sag data obtained from long-term measurements in a real grid. After statistical analysis, the sags' duration and magnitude distributions, and the probability distribution functions were obtained [54]–[57]. Recently, such an approach has been used to develop a stochastic model for forecasting voltage sags in a real grid [58]–[61]. In [58], the stochastic characterization of voltage sag data obtained from long-term monitoring in a Portuguese grid is presented. It is shown that the occurrence of voltage sags as a Poisson process is not valid if voltage

sags clusters (grouped sags) are included. In the opposite case, a gamma distribution fitting was confirmed. In [59], some ideas for voltage sags forecast using the parameter *time to the next event* as the probabilistic variable are given. Further elaboration is provided in [60]. In this paper, a gamma distribution is proposed to properly model voltage sags based on the forecast. High accuracy was achieved, i.e., the forecast presented an error slightly greater than 10%. The method was further improved in [61] by introducing special indices of intermittence to detect and remove grouped voltage sags (clusters). In this case, rare voltage sags can be predicted. The results showed that the rare voltage sag forecast had acceptable errors and was not prohibitive.

However, none of the previously described methods provide predictions in real-time, and they require either knowledge of the grid parameters or long-term measurements. Therefore, they are not suitable for application in the control systems of modern DERs and of the devices for PQ improvement.

III. PROBABILISTIC PREDICTION OF VOLTAGE SAGS DURATION

A. REAL-GRID MEASUREMENT RESULTS ANALYSIS

To define the method for real-time (online) prediction of the probability of the voltage sag duration (RTPP), the authors analyzed various measurement results presented in the literature [3], [40], [54]–[56]. As the most convenient, the available set of real-grid measurement data, measured at different voltage levels and in different distribution grids, containing 680 recordings, out of which 95 were voltage sags, was selected for further analysis. A detailed description of these voltage sags is given in [40], [47]. The main characteristics of these sags and MHDU are presented in Appendix (Tables 6 and 7), while the magnitude-duration graph is shown in Fig. 1. It can be observed that most of the sags end in the period up to 3 s and that they can be regarded as momentary sags (83 sags / 87%). Very few of them have a longer duration (above 3 s), i.e., temporary sags (12 sags / 13%), which follows the previous conclusion regarding the distribution of results. This observation motivated the authors to perform further analyses using the HF to enable real-time sag duration prediction.

B. HARMONIC FOOTPRINT ANALYSIS

All available measurement records were represented using HF characteristics, but only MHDU was considered. The descriptive statistic of HF regarding MHDU for a sample of size N=95 is presented in Table 1. Momentary and temporary sags are distinguished and the mean value of the MHDU and 95% Confidence Interval (CI) of the MHDU were calculated. It can be observed that momentary and temporary sags can be distinguished and that a probabilistic model may be formed. Therefore, we propose the following hypothesis:

Hypothesis: Based on the maximum value of the harmonic footprint (MHDU) during a transient, it is possible to determine the probability that a voltage sag will develop as temporary or momentary.

TABLE 1. real-grid measurements: descriptive statistics of MHDU.

Sag	Number	Mean	95% CI
Momentary	83	14.2673	(12.1;16.44)
Temporary	12	48.8292	(40.12 ;57.54)

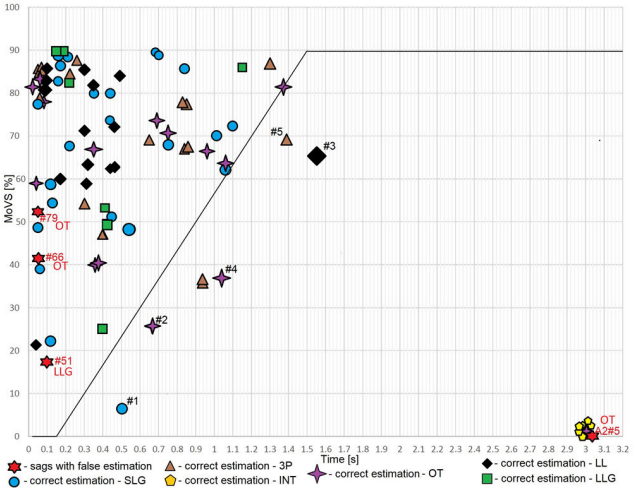

FIGURE 1. Selection of the voltage sag measurement data used for analysis.[2] LEGEND: SLG is a single-line-to-ground fault, LL is line-to-line, LLG is double-line-to-ground, 3P is a three-phase fault, INT is an interruption, and OT is signifying the other type of faults (usually complex disturbances). The solid line represents German grid code limits.

C. MATHEMATICAL ANALYSIS - LOGISTIC REGRESSION MODEL

To treat the hypothesis in this research, among well-known traditional techniques (such as ordinary least squares regression or linear discriminant function analysis), the logistic regression model was chosen. Generally, logistic regression is widely used in modern statistics to test hypotheses where the outcome is a categorical variable (in this case, dichotomous), while predictor variables (one or more) can be categorical or continuous [62]–[65]. In practice, many problems require analysis and predictions based on dichotomous variables [66], [67]. Therefore, the probability that a voltage sag is temporary or not can be computed using the logistic regression model.

Let us indicate with X a random variable, which represents MHDU for a given sag with a set of values from 0% to 100%, and with Y a dichotomous variable, which takes a value of 1 for temporary sags ($\geq$3 s) and 0 for momentary sags ($<$3 s). Then, a probability function of happening Y, for a specific value $X = x$ can be defined as

$$f\,(X = x) = P\,(Y = 1\,|\,X = x) \tag{1}$$

Logistic regression is based on the *logit* function of one or more dependent variables. The *logit* function of $f(X)$ is the natural logarithm (ln) of odds, which represents the ratio of probability $f\,(X) = P$ (when $Y = 1$ for a given value of X)

to probability $1 - f(X) = P$ (when $Y = 0$ for a given value of X), i.e.,

$$logit\,(f(X)) = ln\frac{f(X)}{1-f(X)}. \tag{2}$$

The simple logistic model (with one independent variable X) has the form

$$ln\frac{f(X)}{1-f(X)} = \alpha + \beta X, \tag{3}$$

where α is the constant of the model, and β is the regression coefficient.

Using equation (3) and taking the antilog of both sides, it is obtained

$$f\,(X) = 1 - \frac{1}{1+e^{\alpha+\beta X}} = \frac{e^{\alpha+\beta X}}{1+e^{\alpha+\beta X}}. \tag{4}$$

Therefore, the standard logistic function with one independent variable X is defined as

$$f\,(X) = \frac{e^{\alpha+\beta X}}{1+e^{\alpha+\beta X}} = \frac{1}{1+e^{-\alpha-\beta X}}, \tag{5}$$

where coefficients α and β are estimated from given data.

To calculate the coefficients and further test the performances of the method, the available set of measured data was divided into two groups: main (83 sags) and control (12 sags). Using statistical software Minitab and 95% confidence level (CL), and based on 83 measurements of the main group, the obtained coefficients for the model (presented by (5)) are $\alpha = -9.15$ and $\beta = 0.23202$. The coefficient α is constant and determines the horizontal position of the logistic regression curve. The slope of the curve is specified by coefficient β. As $\beta > 0$, the probability that the sag is temporary rises with the increase in the maximum value of the HF (MHDU).

The graph of the logistic curve, i.e., the probability function of the MHDU, is determined by

$$f\,(X) = \frac{1}{1+e^{9.15-0.23202X}}, \tag{6}$$

and presented in Fig. 2. The fits and diagnostics for all observations are provided in the Appendix (Table 8). As it can be seen, the graph is a sigmoidal (or S-shaped) curve, with probability values tending to 0 for $X < 30$ and 1 for $X > 50$. Thus, this hypothesis was confirmed. However, fine-tuning is required.

D. FINE-TUNING OF THE RTPP

The calculated value $f(X = x)$ is the probability that the sag with *MHDU=x* will develop as temporary, whereas 1-$f(X)$ is the probability that it will be momentary. To obtain fine-tuning of the border (uncertain) zone for the RTPP (Fig. 2), several probabilities were tested in the range of $30\% < X < 50\%$.

As $f(X = 30\%) = 0.1007$, for MHDU values less than 30%, it can be stated that the considered sag will develop as momentary with a probability greater than 90%.

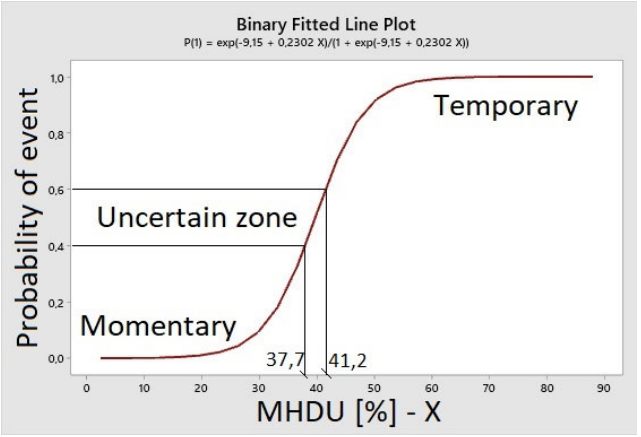

FIGURE 2. Graph of probability function of the Harmonic footprint.

As $f(X = 50\%) = 0.9206$, for MHDU values greater than 50%, it can be stated that the considered sag will develop as temporary with a probability greater than 92%. Moreover, as $f(X = 52.5\%) = 0.9540$, i.e., for MHDU values greater than 53%, the sag will develop as temporary with a probability greater than 95%.

As $f(X = 37.7\%) = 0.4006$, $f(X = 39.5\%) = 0.5073$, and $f(X = 41.2\%) = 0.6009$, the values of the MHDU around 40% are border values, so the probabilities of sag duration are approximately the same and the prediction cannot be exactly obtained. Therefore, the values of the MHDU between 37.7% and 41.2% will be treated as an "uncertain zone," and the probability function curve can be updated (see Fig. 2).

Finally, the effectiveness of the model must be examined.

E. EXAMINING THE MODEL EFFECTIVENESS

There are several ways to examine the effectiveness of a model [68]. In this research, the effectiveness of the proposed model is examined with: 1) significance of predictor coefficient, 2) values of R^2, and 3) measure of goodness-of-fit of the model.

The standard Wald test was used to examine the significance of the predictor coefficients [69]. The proposed null hypothesis for this test is that some coefficients are equal to zero (i.e., no effect in the model). In Table 2, besides the values of constants, the following are presented: 95% confidence interval, Z-values (a statistical measurement that represents a value related to the mean of a group of values), and p-values (the probability of finding the observed, or more extreme results, under the null hypothesis). As the p-values for α (constant) and β (coefficient of X) were less than 0.05, both coefficients were significant in the model. Thus, there is a linear relationship between the *logit(f(X))* and X.

An additional measure for evaluating the performance of the proposed model performs is the coefficient of determination R^2 (pseudo-R-squared). The Cox-Snell R^2 (R^2_{CS}) [70] and Nagelkerke R^2 (R^2_N) [71] coefficients were calculated to

TABLE 2. Coefficients.

Term	Coefficient	95% CI	*Z*-value	*p*-value
Constant (α)	-9.15	(-14.21;4.09)	-3.54	0.000
X (β)	0.23202	(0.0981;0.3623)	3.52	0.001

TABLE 3. Confusion matrix.

Predicted \ Actual	0	1
0	81 (83)	2 (1)
1	2 (0)	10 (11)

be $R^2_{CS} = 0.6881$ and $R^2_N = 0.6742$, respectively. Because these values were greater than 0.5, the model effectively matched the data.

Finally, the goodness-of-fit of the model was verified using the Pearson and Hosmer-Lemeshow test [62], resulting in p-values of 1 and 0.998, respectively. As both p-values are high, the null hypothesis that the observed and expected proportions are the same is accepted, i.e., the presented model (6) fits the given data well.

From the above results, it can be concluded that the model presented in (6) can provide a real-time prediction of the probability of the voltage sag duration based on the HF value of MHDU. Therefore, this hypothesis was confirmed, and the RTPP method could be applied.

F. DISCUSSION

The proposed RTPP method represents a binary classifier, where outputs are "0," i.e., there is a high probability that sag will be "momentary" and "1," i.e., there is a high probability that sag will be "temporary". However, the distribution of these solutions is unequal, and classification accuracy alone can be misleading. Therefore, the confusion matrix was chosen as an adequate technique for summarizing the performance of this classification algorithm [72].

The confusion matrix consists of rows representing the instances in a predicted class and columns representing the instances in the actual class. To fill the matrix, a probability of 0.5, for the trigger value, is chosen, i.e., if $f(X = x) \geq 0.5$, then the sag with MHDU $= x$ is predicted as temporary. The confusion matrix for the proposed model is presented in Table 3. It can be seen that there are only 2 false-positive cases (when momentary sag is predicted as temporary) and 2 false-negative cases (when temporary sag is predicted as momentary). Furthermore, three of those four false cases are in the uncertain zone, while one temporary is classified as momentary.

Considering all recorded signals, for only four (out of 95) duration probabilities could not be determined correctly (95.8% reliability). In Fig.1, they are marked with red hexagrams, with the sag type and number next to the mark.

Thus, it can be concluded that the reliability (success rate) of the algorithm across all recordings was 95.8%. Three out of four sags with incorrect estimations were in the uncertain zone, and for them, the model did not provide any prediction. These three sags were very short, with durations of 0.1 s, 0.05 s, and 0.05 s, respectively. The false estimation of the duration probability is for one temporary interruption because this fault contains multiple disturbances.

IV. THE RTTP ALGORITHM

The RTPP method is a real-time method; therefore it is suitable for implementation in the control system of power electronic converters connected to the grid (grid-tied inverter in the case of DER). A flow chart of the RTPP algorithm is presented in Fig. 3 as part of the control structure for dealing with voltage disturbances and LVRT requests.

The first step in all systems is to acquire three-phase voltage signals in digital form from the voltage sensors (transducers) in the grid. They are converted to a digital form by A/D conversion and sent to the power electronic converter inputs (Va, Vb, and Vc inputs in Fig. 3). The time required for preprocessing is normally not included in the voltage sag detection time, as it is usually much shorter. For example, the Hall voltage sensor response and A/D conversion time may be estimated to be less than 0.24 [ms].

The calculation procedure for the RTPP determination starts with the transformation of digital voltage signals from the time to the frequency domain using one of the well-known methods of time-frequency transform (DFT, RFFT, SFTF, or other). From the transformed signal (in the frequency domain), a specific set of low-order harmonic amplitudes are extracted (2^{nd}, 3^{rd}, 5^{th}, and 7^{th} harmonics), and HF (or HDU2357) is calculated. An HF pattern was formed (sample-by-sample) and its characteristics were determined.

The first monitored samples were treated using a neural network (NN) to obtain the early detection of voltage sags, as presented in [40]. If the sag is detected, then the disturbance mode is activated.

The next step was to determine the maximum value of the HF or MHDU. The MHDU is typically reached in the first half-cycle of a fault (10 ms), therefore this parameter can be obtained in the 10-15 ms range. It can be used to predict two sag characteristics: magnitude and duration.

For magnitude (MoVS) prediction, the method presented in [46] was used. In this case, LVRT requirements can be fulfilled, and the DER may function in the grid supporting mode.

For the prediction of duration probability, which is the topic of this paper, the obtained value of $MHDU{=}x$ is inserted in (6), and the probability of voltage sag duration is calculated ($f(X = x)$). The sag is then predicted as "momentary" or "temporary" using the S-curve shown in Fig.2.

The algorithm for RTPP determination and duration anticipation, as described above, is shown in Fig. 3. Together with other blocks, the method may be used as a pre-control block in an inverter control system for operation in cases of voltage sags.

V. APPLICATION OF THE RTTP METHOD

A. APPLICATION OF RTPP FOR GRID-TIED INVERTER

The RTPP method, together with methods for voltage sag detection and MoVS prediction, are applied to the grid-tied

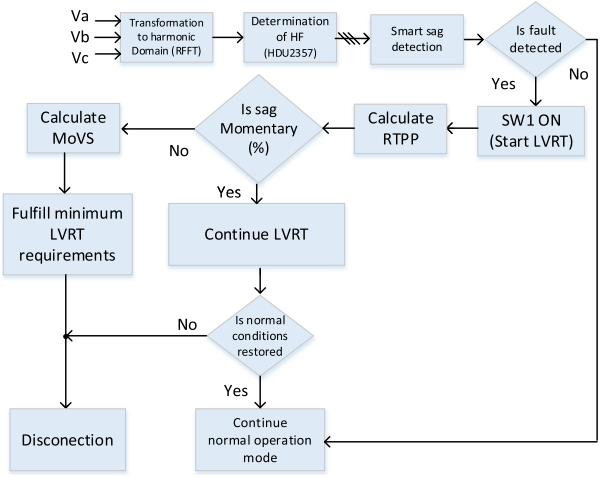

FIGURE 3. Flowchart of RTPP with smart detection and MoVS prediction.

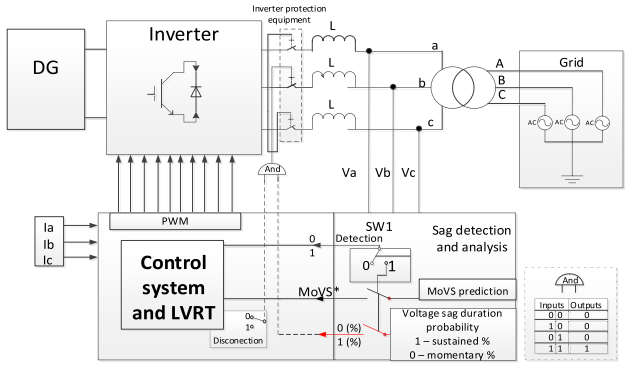

FIGURE 4. The simplified overall structure of grid-connected DG system, with an application of the RTPP algorithm, together with fast detection and MoVS prediction algorithm.

inverter control used for the DER (Fig. 4). The control system of the DER (including LVRT control) is modeled according to [73] and further modified with a pre-control block, which includes sags detection, MoVS prediction, and the RTPP subblocs, together with additional digital switches (as shown in Fig. 4).

In the detection block, the HF is calculated, and if sag is detected, the digital switch (SW1) is turned on. For voltage sag detection, smart algorithm based on HF using Recurrent neural network is used, as described in [40]. The maximum value of HDU2357 (MHDU) can be then determined. The value of MHDU is used in the RTPP algorithm; therefore, the voltage sag duration can be predicted to be momentary or temporary with corresponding probability. In addition, MoVS is predicted.

Based on the categorization results (momentary or temporary) and following the estimated MoVS values, further actions are taken regarding the operation in the LVRT mode. If the fault duration is predicted to be momentary and if MoVS is below the LVRT line, the disconnection will be delayed. Delay is set to be in the range of 0.3 s - 1.5 s, depending on MoVS, and an extended LVRT control strategy can be determined, together with appropriate references for

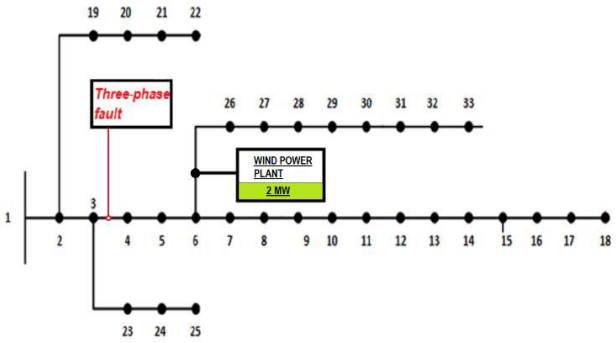

FIGURE 5. Simplified diagram of the modified IEEE33-bus test grid.

P and Q generation during the sag. In addition, information about the expected voltage levels during a fault is known after around 10 ms. Based on the requirements of IEEE Std. 1547-2018 and/or relevant grid-code, the minimum duration of LVRT support (before DG disconnection) can be approximately determined. The RTPP algorithm was designed to enable duration estimation at the beginning of the fault.

B. APPLICATION OF RTPP FOR GRID-TIED INVERTER IN THE MICROGRID HIL LABORATORY TESTBED

The complete method was further applied to the Microgrid Typhoon-HIL testbed in the Laboratory of Typhoon-HIL in Novi Sad, on the Typhoon HIL604 real-time emulator. The Typhoon HIL Control Center (THCC) program package was used together with the Schematic Editor and HIL SCADA subsystems. The power production during LVRT and the operation of the protective and switching equipment are controlled externally using an algorithm that includes the RTPP method.

The IEEE 33-bus grid was adapted with a 2 MW wind turbine. It consists of 33 bus bars (three-phase nodes) arranged on 4 main feeders. Each line connecting the nodes was 1 km long. The nodes are connected to 32 three-phase lines. The loads are connected to each of the 33 nodes. The source of the grid is a generator (component ''Grid'') that represents a balance node, a three-phase source, of the nominal voltage of 12.66 kV, which can generate the necessary amount of energy to sustain voltage. All other nodes (considering the power flow angle) are P/Q types. The total active power was 3.715 MW, whereas the total reactive power was 2.3 MVAr. The system is operating at a frequency of 60 Hz. A simplified diagram of the modified IEEE33-bus test grid is shown in Fig. 5.

A generic wind turbine, which is located within the microgrid subgroup in Library Explorer, was selected for the distributed power source in this system. The wind turbine is connected to the network between nodes 706 (node 6) and 726 (node 26) using a transformer of 0.4/12.66 kV/kV.

The Microgrid Typhoon-HIL testbed that is used for laboratory testing is shown in Fig. 6. The main part and the ''brain'' of the setup are Typhoon HIL 604 devices (three devices, marked in Fig. 6 with numbers 1, 4, and 6), which

FIGURE 6. Microgrid Typhoon-HIL testbed.

are used in the HIL emulation procedures. Below, there is the generator controller the Woodward easYgen-3500 (marked as 2). The SEL-751 relay (marked as 3), which is used to protect feeders in radial and tangled distribution networks is under it. Next in line, is another HIL 604 device (marked as 4), which is connected to the Typhoon HIL Connect device below it (marked as 5). The HIL Connect is used to interface the controller with the existing HIL system. Below is another HIL 604 (marked as 6), which is connected to a Typhoon HIL EPC Power controller (marked as 7).

C. APPLICATION OF RTPP IN THE FIELD OF PROTECTION

The method of voltage sags characterization using HF also has some advantages in the field of protection. The use of fast voltage sags detection in microprocessor relay operations has been reported [74].

The application of the proposed RTPP algorithm enables swift prediction in a period far below the normal reaction time of the protection relays. For example, the preprocessing stage (Hall voltage sensor response and A/D conversion) may be estimated to be less than 0.24 [ms], while the RTTP of additional 10-15 [ms]. However, false detection can lead to undesired disconnection of the DER or unselective/unwanted protection equipment operation. For example, the starting of induction motors and transformer energizing do not require the operation of a protection system, but they may be mistaken for sags caused by faults [46]. Therefore, it may have value in a modern microgrid for proper coordination between the protection system and LVRT requirements of the DERs [75]. In our simulation and experiment, we included the LVRT requirements, but relay tripping was not considered.

VI. TESTING OF THE PROPOSED METHOD

The proposed RTPP method is based on the HF feature of the voltage sag, i.e., on implementation of the sag's MHDU value. As mentioned previously, a set of real grid measurement results was used to support the method. Their HF parameters were determined and are presented in [46], where a strong correlation between the MHDU and MoVS was observed. In this paper, it is shown that by using the same measurement results and MHDU values, the voltage sag duration can be predicted with high probability. Complete tables with the test results are provided in the Appendix. In Tables 6 and 7 types of faults, the magnitude of voltage sag (MOVS), duration of fault, and maximum of harmonic footprint (MHDU) result are presented for momentary and sustained disturbances, respectively. In Table 8, the fits and statistical parameters for all real grid measurements are shown.

A. TEST SETUP – MODIFIED IEEE 13-BUS TEST GRID

To test the RTPP algorithm, real grid measurement data were applied to a distribution network model. The aim was to determine the benefits of the algorithm to the voltage supply of residential consumers. A modified IEEE13-bus test grid with a total of 3.25 MW of added DER generations (two PVs of 1.25 kW and one wind plant of 2 MW) and 0.464 kVA of residential area load was used. The IEEE13-bus test grid is a reduced model of an unbalanced real grid; therefore, with applied real-grid (in-field) measurement data, appropriate emulation of real grid cases may be achieved.

A simplified diagram of the modified IEEE13-bus test grid is shown in Fig. 7. A 2 MW wind plant consisting of four 0.5 MW wind turbines was added at a location 1 km from bus #633 (close to the distribution transformer). Wind turbines are doubly-fed induction generators (DFIGs) with an AC/DC/AC IGBT-based PWM voltage source converter (VSC). A 1 MW PV plant with a grid-tied inverter (DC/AC converter) was connected to the #652 bus through a 2 km line. A residential area with an added total of 0.25 MW roof-top PV systems and a total load capacity of 0.494 kVA was connected to the #634 bus.

B. TEST RESULTS WITH EMULATED REAL-GRID SAGS

The algorithm was tested using emulated real-grid measurement results, i.e., assuming that such voltage sags were recorded at the observed bus #634. A critical distance method was used to detect the location of faults in the IEEE 13-bus test grid [48], [49]. The faults are located around buses #632 (Fault Location 1, FL1) and #648 (FL2) and close to bus #692 (FL3), as indicated in Fig. 7. Therefore, the voltage sags at bus #634 resulting from faults in the grid have the same parameters (magnitude and duration) and time waveforms as the sags obtained from the recorded real-grid measurements (Fig. 1).

For testing, six voltage sags were selected corresponding to the ones shown in Fig. 1. They are outside or on the line of the German grid code minimum requirements for the LVRT, i.e., of such duration (0.41 s - 1.55 s) and magnitude that they would probably cause a DER disconnection. The selected sags were regenerated using the detected fault locations in the test grid model and the appropriate fault parameters. For example, for fault #1, the parameters are fault

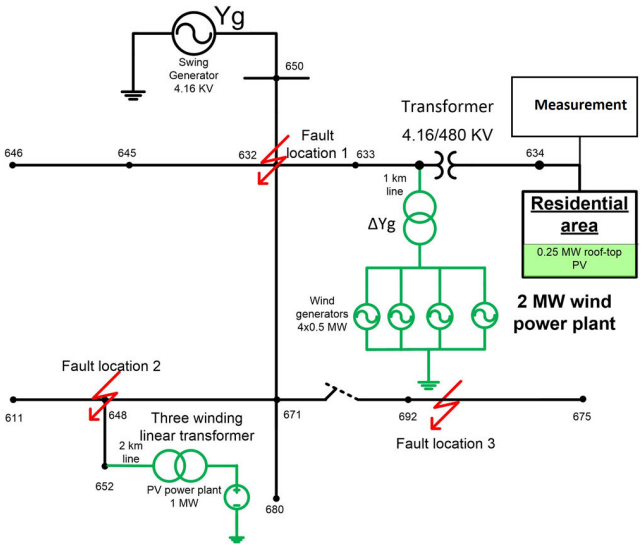

FIGURE 7. Simplified diagram of the modified IEEE13-bus test grid.

TABLE 4. Measurement and test results.

No.	Type & location	Duration [s]	MoVS [%]	MHDU [%]	RTPP *f(X=x)*	TG [s]
#1	SLG at FL1	0.41	0 / 9	31.8	0.1453	0.41
#2	OT at FL1	0.67	0 / 29	28.3	0.0702	0.66
#3	LL at FL2	1.55	58 / 68	15.3	0.0037	1.54
#4	OT at FL3	1.06	17 / 27	29.6	0.0926	1.04
#5	3P at FL3	1.39	56 / 71	16.5	0.0049	1.36
#6	SLG at FL2	0.54	28 / 52	21	0.0137	0.53

LEGEND: LL is a line-to-line fault, SLG is a single-line-to-ground fault, 3P is a three-phase fault, and OT is another type of fault.

resistance 0.0001 Ω, ground resistance 0.001 Ω, fault/sag duration 0.41 s, and voltage sag MoVS 6.35%. The fault number, type, location, and parameters (duration and magnitude-MoVS (left number)) are presented in Table 4. Voltage sag #1 is shown in Fig. 8, sag #6 in Figs. 9 and 10, whereas the others are omitted because of lack of space. Simulation is building up at the start, and steady-state is reached at 0.05 s, so results from 0 s to 0.05 s may be discarded. The faults were generated at 0.09 s.

The values of the obtained MHDU and RTPP for all the six tested faults are presented in Table 4. The first (left) MoVS value is obtained when all DERs are disconnected (without RTPP), whereas the second (right) is obtained if they are active in the LVRT mode because of the RTPP usage. It can be observed that all MHDU values are below the limit of 37.7% (see Fig. 2); therefore, their RTPP is low, and all sags are anticipated to be momentary. Results show that for all six cases the RTPP algorithm successfully predicts duration as ''momentary'' with probability in the range from 85.47% for the fault (sag) #1, up to 99.63%, for the fault (sag) #3.

A graphical representation of the test results for fault #1 (SLG) is presented in Fig. 8. In Figs. 8 (a) and 8 (b), the line voltages at bus #634, with and without the integrated RTTP algorithm are presented, respectively. As shown in Fig. 8 (b),

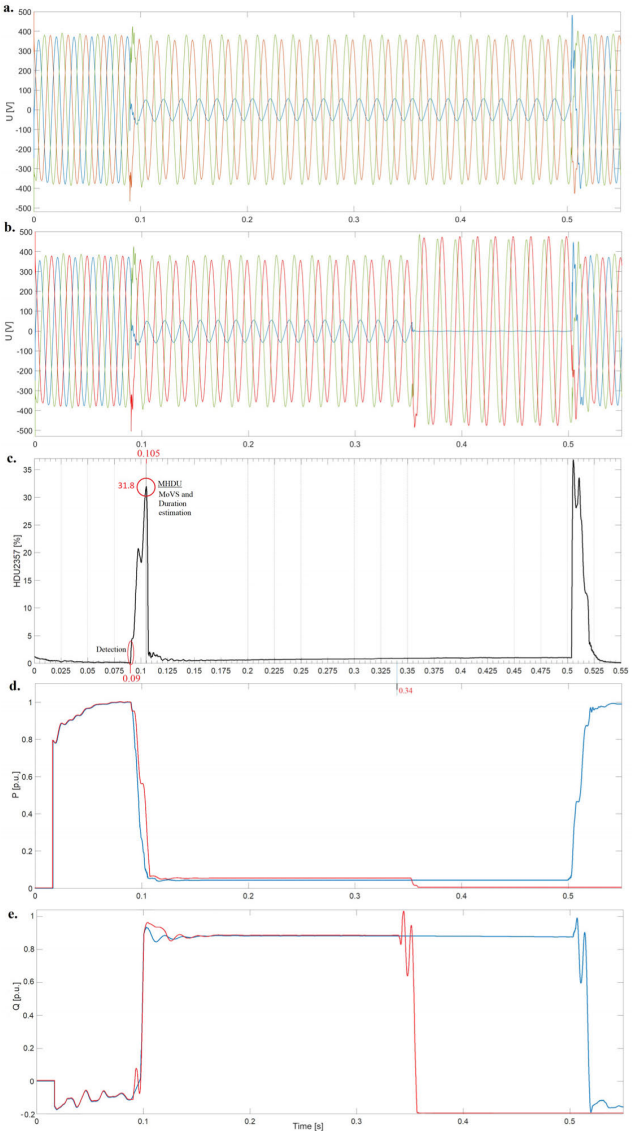

FIGURE 8. Results for Fault #1 from Table 4: (a) Voltages at bus #634 and DER control with RTTP; (b) Voltages at bus #634 and DER control without RTTP; (c) Harmonic footprint; (d) Active power (P) of the wind plant with the proposed algorithm (blue line) and without it (red line) in phase with the fault; (e) Reactive power (Q) of the wind plant with the proposed algorithm (blue line) and without it (red line) in phase with the fault.

after 0.36 s the DERs are disconnected, following the LVRT minimum requirements from the German grid code. On the other hand, Fig. 8 (a) shows that the DER disconnections are prevented owing to the application of the proposed algorithm. In Fig. 8 (c), the harmonic footprint is presented with the important points indicated. The starting voltage sag's transient and ending transient can be distinguished. MHDU value (31.8%) can be observed, so the sag is predicted as ''momentary.'' Subsequently, the LVRT mode is activated, and the DERs support the grid; therefore, the voltage magnitudes during the sags at bus #634 are higher.

In Figs. 8 (d) and 8 (e), the active (P) and reactive (Q) power of the 2 MW wind farm with the proposed algorithm (blue

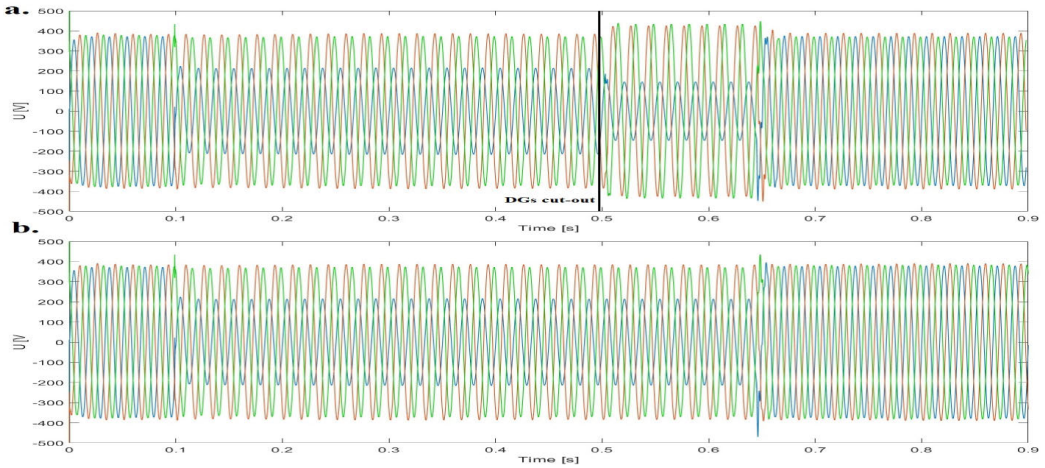

FIGURE 9. Simulation results for Fault #6 from Table 4: (a) Voltage signals at a residential area in bus #634 without the RTPP algorithm; (b) Voltage signals at a residential area in bus #634 with the algorithm for the RTPP.

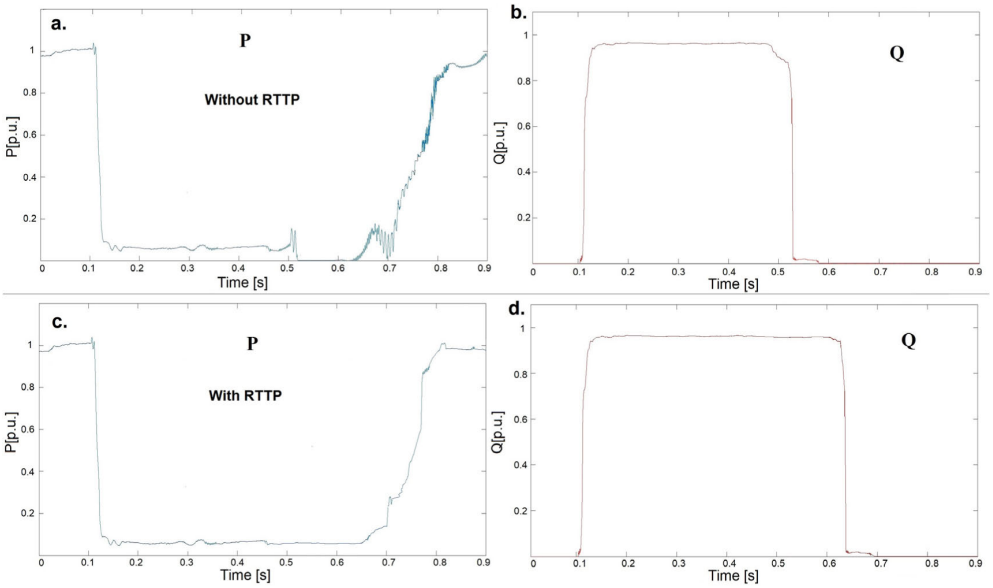

FIGURE 10. Simulation results for Fault #6 from Table 4, the P and Q production of 2 MW wind plant in [p.u.]: (a) Active power production of the wind power plant without the algorithm for RTPP; (b) Reactive power production of the wind power plant without the RTPP; (c) Active power production with the RTPP; (d) Reactive power production with the RTPP.

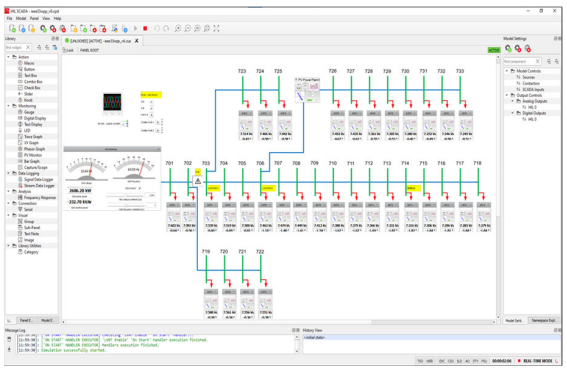

FIGURE 11. SCADA control during emulation using the HIL laboratory setup.

line) and without (red line) are presented, respectively. The wind farm was chosen because it has the highest power. The responses of PV plants were similar. The grid support criteria are defined by LVRT requirements, which may differ from country to country [22]. Usually, it is required to generate both P and Q if voltage during the sag is above 50% of the rated, and the Q only if it is less. It can be seen that the DER continues to support the grid, so voltages at bus #634 are better and DER operation is not disrupted.

In Fig. 9, another example of voltages in a residential area during a voltage sag in the grid is presented (single-phase to ground). The simulated sag, with a magnitude of 52.8 %, following IEEE Std. 1547-2018 again belongs to the group of sags where DGs have permissive operation capability up to 0.3 s of duration. This time, the DGs are disconnected at 0.49 s after the sag duration of 0.4 s. Immediately, voltage further drops to 35.6% (i.e., for an additional 17.2%), causing transient and harmonic bursts in the grid. In addition, in the

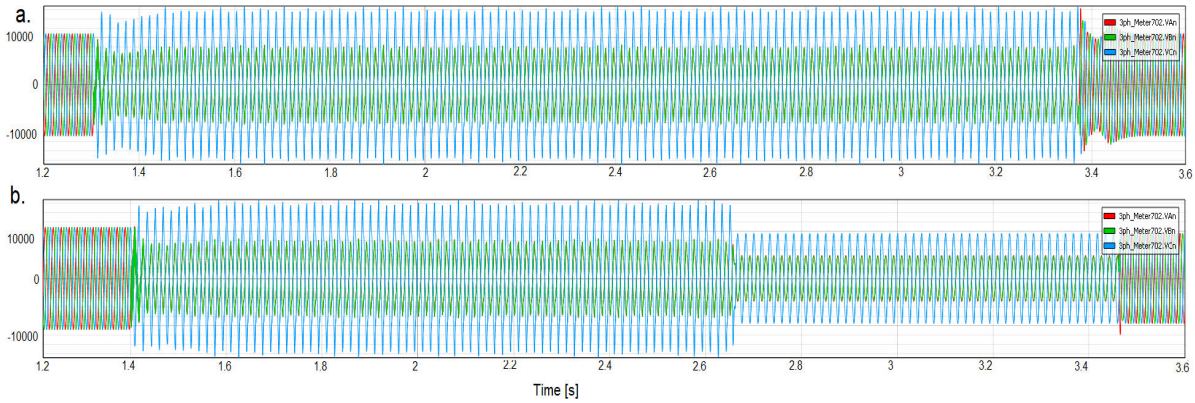

FIGURE 12. Results of laboratory testing on Microgrid HIL testbed for the fault #1 from Table 5: (a) Voltages at Wind turbine and DER control with RTTP; (b) Voltages at Wind turbine and DER control without RTTP.

TABLE 5. Test results on laboratory microgrid HIL testbed.

Fault No.	Type & location	Duration [s]	MoVS [%]	MHDU [%]	RTPP *f(X=x)*	TG [s]
#1	LLG	2	43 / 71	10.8	0.0013	1.98
#2	OT	0.7	4 / 25	27.8	0.0629	0.69
#3	SLG	0.96	41 / 55	25.3	0.0363	0.95
#4	3PG	40	5 / 13	60	0.99	39
#5	SLG	0.8	31 / 42	36	0.1	0.78

other two phases, after DGs cut-out, an immediate increase in voltage can be observed, causing voltage swells in these phases.

In Fig. 10, the P and Q productions of the 2 MW wind power plant during a fault in the grid (fault #6 from Table 4) are presented. In Figs. 10. (a) and 10. (b), the P and Q values without implementation of the RTPP algorithm in the control system of the inverter are presented, whereas in Figs. 10. (c) and 10. (d), the same values are shown with the use of the RTPP algorithm. It can be observed from Figs. 10. (c) and 10. (d) that with the application of the algorithm presented in this paper, unnecessary tripping of the 2 MW wind power plant is avoided, and immediately after recovery of the voltage, normal power production is restored.

As MoVS during sag is 53%, according to [23], the production of active power during LVRT should be close to zero, and almost all delivered power should be reactive to support the voltage. The inverter control in the simulation was modeled following these recommendations.

C. TEST RESULTS WITH TYPHOON-HIL SETUP

The algorithm was further tested in a laboratory HIL environment using an advanced Typhoon-HIL Microgrid setup. For testing, five voltage sags were simulated in the modified IEEE 33-bus test grid. Faults were set to be located between buses #2 and #3 (Fig. 6). The measurements were performed at the interconnection point of the wind turbine to the grid. The results are presented in Table 5. It can be observed that all MHDU values are below the limit of 37.7% (see Fig. 2) and that all sags are anticipated to be momentary.

As shown in Fig. 11, the SCADA window is made up of a graphical representation of the IEEE 33 bus network, in which each node has a special sub-window showing the value of the phase voltage, as well as the phase shift relative to zero nodes. At the root of the network, there is a window that enables the setting of the grid component's voltage reference value and frequency as well as tracking these values, along with the active and reactive power of the network.

In Fig. 12, the line voltages for two cases, when the wind power plant control is with the integrated RTTP algorithm and without it, are presented. In Fig. 12 (a), it is shown that the DER disconnection is prevented by the application of the proposed algorithm. On the other hand, in Fig. 12 (b), it can be seen that after 1.25 s the DER is disconnected, following the LVRT minimum requirements from the German grid code, so another voltage transient followed by a further decrease in voltage can be observed. Figs. 12 (a) and 12 (b) are not aligned, and the starting time of recording of signals and the end time are not the same, as the testing is performed in real time. Similar to Fig. 12, the test results from the HIL testing are presented for Fault #5 in Fig. 13. In Fig. 13 (a) DER disconnection is prevented due to operation of the RTPP, while in Fig. 13 (b) it can be seen that after 0.72 s the DER is disconnected. Fig. 13 (c) shows the HDU2357 values during the voltage sag.

The results show that for four cases the RTPP algorithm successfully predicted the duration to be ''momentary'' with probability in the range from 90% for sag #5, up to 99.87% for sag #1, and sag #4 is successfully predicted to be ''temporary'' with the probability of 99%.

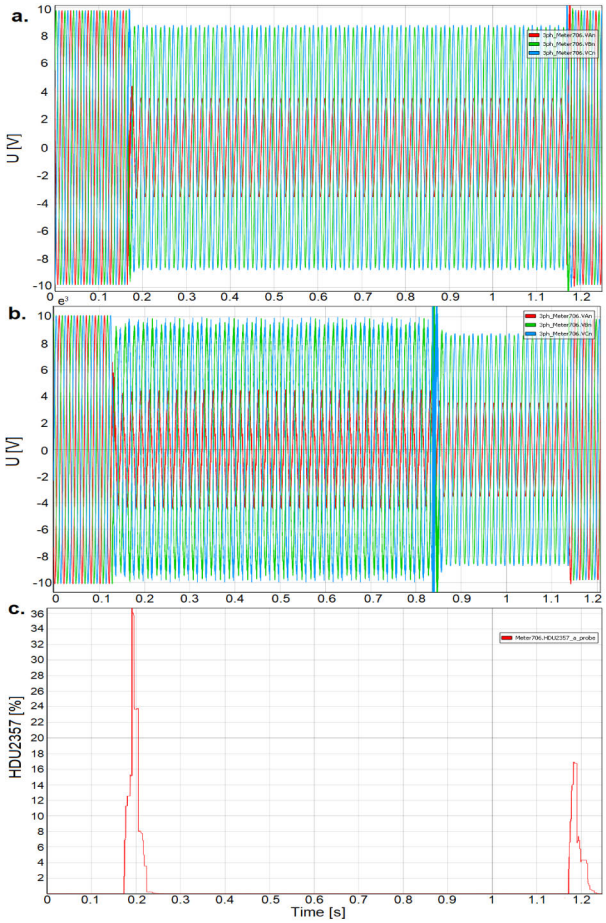

FIGURE 13. Results of laboratory testing with Microgrid HIL testbed for Fault #5 from Table 5: (a) Voltages at the wind plant including the control with the RTTP; (b) Voltages at the wind plant without the RTTP; (c) HDU2357.

D. DISCUSSION

In Fig. 1, German grid code limits were added to indicate the minimum requirements for LVRT operation. They defined that a DER should support the grid within a certain period and then disconnect if a fault is not cleared. Considering the case of Fault #1 shown in Fig. 8, it should be at 0.25 s from the start of disturbance, that is, at 0.34 s (Fig. 8 (b)). Immediately after disconnection (0.36 s), the voltage magnitude dropped to zero (Fig. 8 (b), blue line). In addition, after the DERs cut-off, an immediate increase in voltage can be observed, causing the voltage to swell in other non-faulted phases.

The voltage diagrams in Fig. 8 (a) show that with the implementation of RTPP, the sag duration is predicted as ''momentary''. This information is provided to the adapted control algorithm, which enables additional time for LVRT support - from 0.34 s to 0.5 s. At the 0.5 s, the voltage sag ends, voltage is recovered, and the DERs continue their normal operation without tripping.

Furthermore, similar results were obtained during laboratory testing with the Microgrid HIL testbed. The voltage

TABLE 6. Types of faults, the magnitude of voltage sag (MoVS), duration of fault, and maximum harmonic footprint (MHDU) result for momentary disturbances.

No.	Type of fault and short description	MoVS [%]	Duration [s]	MHDU [%]
1	Type G, five cycles, develops into Type A, 60 cycles	86.60	1.3	4.90
2	Type C, 15 cycles, characteristic phase-angle jump about -7 degrees. fault develops from single-phase to two-phase-to-ground	92.30	0.41	5.25
3	Type C, 15 cycles, phase-angle jump	92.60	0.4	7.88
4	multistage Sag, developing fault	51.00	0.45	18.6
5	unbalanced Sag with strange recovery: motor+transformer	60.00	0.17	14.55
6	Type C, 12 cycles, phase-angle jump, very constant rms voltage	72.00	0.46	15.55
7	A remarkable multiple event, no clear explanation. Starts as type C, slow recovery after a few cycles; full recovery; one phase up, two phases down; a repeat of the first event but now with sharp recovery. Line voltages are plotted.	62.00	1.06	19.73
8	Type C, 10 cycles, phase-angle jump, very constant rms voltage	83.87	0.22	7.20
9	Three-phase fault; about 70 cycles long, about -50 degrees phase-angle jump.	25.00	1.56	35.71
10	Three-phase fault, about 20 cycles long, small phase-angle jump	88.57	0.39	4.55
11	Voltage Sag with overvoltage in one phase, possible two-phase-to-ground fault	91.00	0.18	3.24
12	two phases down, one phase up, 6 cycles	89.03	0.17	3.21
13	Voltage Sag with overvoltage in one phase, possible two-phase-to-ground fault	82.54	0.22	7.50
14	Type C, 18 cycles, small phase-angle jump, small load effect	49.30	0.41	25.14
15	Type C, 15 cycles develop into Type G 2 cycles. Single-phase to Two-Phase-to ground. Line voltages are measured.	53.30	0.41	21.29
16	Type D, 30 cycles, faulty operation of circuit breaker leading to waveform distortion during the event.	73.70	0.69	9.44
17	Short Sag, probably a self-clearing fault	59.00	0.04	27.16
18	Type D , no jump, 2-stage recovery	82.67	0.16	7.37
19	Type C, 11 cycles developing into type A 6 cycles with 2-stage recovery. Line voltage is measured	25.05	0.40	29.42
20	Three-phase fault, the difference in recovery instant in the three phases.	53.62	0.33	14.29
21	Type C,11 cycles developing into type A, 3 cycles. With phase-angle jump.	58.86	0.31	15.20
22	Type F, 15 cycles, developing into type A, 15 cycles.	86.00	1.15	4.80
23	Three-phase fault, small phase-angle jump.	87.11	0.26	4.38
24	Three-phase fault with the fluctuating difference between the phase voltages. Two-stage recovery. Fluctuation is not found back in symmetrical components. Looks like an interesting case.	46.80	0.40	22.90

TABLE 6. *(Continued.)* **Types of faults, the magnitude of voltage sag (MoVS), duration of fault, and maximum harmonic footprint (MHDU) result for momentary disturbances.**

25	***Type C, 16 cycles, moderate phase-angle jump, complicated recovery***	***62.86***	***0.46***	***13.91***
26	Type C, 10 cycles, phase-angle jump, some load effect	62.48	0.44	11.27
27	Type C, 15 cycles, phase-angle jump	63.53	0.32	13.20
28	Sag due to single-phase fault, with overvoltages in non-faulted phases.	22.20	0.12	30.73
29	Sag due to single-phase fault, with overvoltages in non-faulted phases.	58.71	0.12	16.71
30	Sag due to single-phase fault, with overvoltages in non-faulted phases.	89.76	0.16	5.08
31	Type C, 25 cycles, no phase-angle-jump, constant rms voltage	83.96	0.49	7.20
32	Unbalanced Sag (Type C) with heavy machine infeed during the start of Sag. Two-stage recovery. Slow recovery after the fault.	71.09	0.30	9.49
33	Unbalanced Sag (Type C) with heavy machine infeed during the start of Sag. Two-stage recovery. Sustained reduced voltage after the fault. Possibly stalling induction machines.	67.00	0.35	11.10
34	Developing fault	25.67	0.67	17.00
35	Type B, 5 cycles (overvoltage) develops into type E (overvoltage), 3 cycles.	86.19	0.17	5.29
36	Type C, 40 cycles, moderate phase-angle jump	67.74	0.75	12.57
37	Type C, 10 cycles, moderate phase-angle jump	67.62	0.22	13.94
38	Type C, 2 cycles developing into Type A, 10 cycles. Includes phase-angle jump	85.62	0.30	7.19
39	Single-phase fault with overvoltages in the non-faulted phases. Two-stage recovery.	48.41	0.54	18.99
40	Same as ZQ483 but closer to the fault location. Voltage in faulted phase is lower initially, but less after the first stage fault clearing.	6.35	0.50	33.65
41	Type C or D, large phase-angle jump, 50 cycles. Phase-angle jump about -18 degrees in one phase, non at all in the two other phases.	72.10	1.10	12.20
42	Type C, 3 cycles, large phase-angle jump. Characteristic phase-angle jump -10 degrees.	77.62	0.05	10.33
43	Type C, 7 cycles develops into Type G, 7 cycles	40.00	0.36	13.56
44	Type D_c, 2 cycles. Characteristic phase-angle jump about -40 degrees.	39.05	0.06	26.30
45	Type F, 15 cycles. Characteristic phase-angle jump: -40 degrees. Transformer saturation between the non-faulted phases.	40.47	0.38	27.18
46	Type C, 15 cycles developed into Type A 15 cycles.	65.40	1.55	12.85
47	Three-phase fault, about 2 cycles load influence at the beginning. Large phase-angle jump.	69.19	1.39	16.49
48	Three-phase fault, about 2 cycles load influence at the beginning. Small phase-angle jump.	77.33	0.85	8.07
49	Three-phase fault, very constant RMS voltage. Phase-angle jump increases from -2 to -5 degrees during the fault.	77.17	0.84	8.56
50	shallow balanced Sag with slow recovery; -3 degrees phase jump, probably distribution fault	93.23	0.30	2.45

TABLE 6. *(Continued.)* **Types of faults, the magnitude of voltage sag (MoVS), duration of fault, and maximum harmonic footprint (MHDU) result for momentary disturbances.**

51	Type F, 5 cycles. Characteristic phase-angle jump -55 degrees.	17.23	0.10	37.50
52	Self-clearing fault: two phase --> single phase --> cleared, all in about two cycles	78.16	0.08	29.25
53	Type D develops into Type A after about 5 cycles	81.30	1.37	6.92
54	Type D, about 16 cycles	89.05	0.68	4.05
55	Recovery after a long three-phase fault developed from a two-phase-to-ground fault	90.40	0.84	3.99
56	Type C, 4 cycles, small phase-angle jump, significant load effects	90.58	0.70	3.83
57	Type C, 4 cycles, small phase-angle jump, significant load effects	90.91	0.21	4.03
58	Type C, 4 cycles, small phase-angle jump, significant load effects	81.30	0.09	7.15
59	Type C, 4 cycles, small phase-angle jump, significant load effects, two-stage recovery	85.16	0.09	6.20
60	Type C, 4 cycles, small phase-angle jump, significant load effects	82.10	0.09	6.88
61	Long developing fault, from single-phase to three-phase, with strong induction-machine infeed at the beginning of every new stage.	66.36	0.96	5.45
62	Sag due to single-phase fault, with overvoltages in non-faulted phases.	54.44	0.13	14.77
63	Three-phase fault, about 5 cycles motor contribution at the start of Sag. Phase angle jump about -5 degrees, slightly larger during the motor contribution	66.84	0.84	8.94
64	Three-phase fault, about 5 cycles motor contribution at the start of Sag. Phase angle jump about -5 degrees, slightly larger during the motor contribution.	67.06	0.85	9.88
65	Type C, five cycles, develops into type A, 15 cycles. Instable RMS voltage.	73.75	0.44	14.98
66	**Very short Sag, hard to say what it is. It may be a measurement error.**	**41.39**	**0.05**	**40.27**
67	Type D, 15 cycles; Type F, 30 cycles, Type A, 5 cycles, long developing fault	36.99	1.04	12.73
68	Three-phase fault, with strange transient in the middle. It may be a measurement error.	36.00	0.94	31.06
69	A few cycles of transient voltage suppressants and noise. It may be a fault that doesn't fully develop.	84.86	0.08	15.30
70	Three-phase fault, with some strange spikes. It may be a measurement error.	35.69	0.94	32.80
71	Fault develops in one cycle. Starts as a phase-to-phase fault; the third phase joins one cycle later.	21.39	0.04	30.08
72	Two-cycle three-phase fault, with a rather slow recovery. No phase-angle jump.	78.32	0.06	7.78
73	Two-cycle three-phase fault, no phase-angle jump.	85.31	0.05	5.41
74	Two-cycle three-phase fault	84.43	0.06	5.76
75	Two-cycle three-phase fault	84.35	0.06	5.92
76	Two-cycle three-phase fault	85.66	0.06	5.36
77	Type C, 25 cycles, two-stage recovery	80.67	0.35	8.93
78	Three-phase fault; Appears to have a large and increasing fault impedance.	68.74	0.65	18.91

TABLE 6. *(Continued.)* **Types of faults, the magnitude of voltage sag (MoVS), duration of fault, and maximum harmonic footprint (MHDU) result for momentary disturbances.**

79	**Short Sag, probably a self-clearing fault**	**52.43**	**0.05**	**47.62**
80	Interesting series of transients/very-short Sags followed by a small upward step in RMS voltage.	81.39	0.02	23.60
81	Type C, 30 cycles, no phase-angle jump, two-stage recovery.	80.08	0.35	8.75
82	Type C, 30 cycles, no phase-angle jump, two-stage recovery.	80.13	0.44	9.14
83	Type C, 10 cycles develop into Type A, 30 cycles. Instable RMS voltage during three-phase fault.	70.79	0.75	16.78

TABLE 7. **Types of faults, the magnitude of voltage sag (MoVS), duration of fault, and maximum harmonic footprint (MHDU) result for sustained disturbances.**

No.	Type of fault and short description	MoVS [%]	Dura-tion [s]	MHDU [%]
84	Interruption after unbalanced fault	0	>3	42.50
85	Non-fault interruption, overvoltage at start	0	>3	55.51
86	Non-fault interruption, overvoltage at start	0	>3	87.88
87	**Non-fault interruption with decay due to motor load**	**0**	**>3**	**37.84**
88	**Multiple disturbance. Sag due to single-phase fault, instability, interruption. It may be unintentional islanding**	0	**>3**	**24.66**
89	Non-fault interruption with decay due to motor load	0	>3	50.03
90	Non-fault interruption with decay due to motor load	0	>3	48.43
91	Non-fault interruption	0	>3	47.28
92	Transients of increasing amplitude, followed by interruption	0	>3	45.72
93	Transients of increasing amplitude, followed by interruption	0	>3	42.68
94	Type C, 5 cycles, more-or-less normal voltage during 5 cycles, non-fault interruption with large overvoltages at the beginning.	0	>3	62.27
95	Non-fault interruption with some small amount of voltage remaining between two phases	0	>3	41.15

diagrams in Figs. 12 (a) and 12 (b) show similar behaviors to those presented in Figs. 8 (a) and 8 (b). After 1.25 s from the start of the disturbance (MoVS 71%), the DER is starting to disconnect from the grid (Fig. 12 (b)). Immediately after disconnection, the voltage magnitude decreased further to 43%. In Fig. 12 (a), it can be observed that with the RTTP algorithm the wind power plant continues the LVRT operation without tripping, and the voltage levels are stable throughout the entire sag.

Without this algorithm, a DER would be disconnected, and the grid support would be terminated. Therefore, some

TABLE 8. **Fits and diagnostics for all observations.**

Obs	MHDU	Obs. Pro.	Fit	Resid	Std Resid
1	4,90	0,0000	0,0003	-0,0257	-0,03
2	5,25	0,0000	0,0004	-0,0267	-0,03
3	7,88	0,0000	0,0007	-0,0362	-0,04
4	18,60	0,0000	0,0077	-0,1240	-0,12
5	14,55	0,0000	0,0030	-0,0779	-0,08
6	15,55	0,0000	0,0038	-0,0874	-0,09
7	19,73	0,0000	0,0099	-0,1412	-0,14
8	7,20	0,0000	0,0006	-0,0334	-0,03
9	35,71	0,0000	0,2840	-0,8174	-0,84
10	4,55	0,0000	0,0003	-0,0247	-0,02
11	3,24	0,0000	0,0002	-0,0212	-0,02
12	3,21	0,0000	0,0002	-0,0211	-0,02
13	7,50	0,0000	0,0006	-0,0346	-0,03
14	25,14	0,0000	0,0336	-0,2616	-0,27
15	21,29	0,0000	0,0141	-0,1688	-0,17
16	9,44	0,0000	0,0009	-0,0433	-0,04
17	27,16	0,0000	0,0525	-0,3284	-0,33
18	7,37	0,0000	0,0006	-0,0341	-0,03
19	29,42	0,0000	0,0853	-0,4222	-0,43
20	14,29	0,0000	0,0029	-0,0756	-0,08
21	15,20	0,0000	0,0035	-0,0839	-0,08
22	4,80	0,0000	0,0003	-0,0254	-0,03
23	4,38	0,0000	0,0003	-0,0242	-0,02
24	22,90	0,0000	0,0204	-0,2028	-0,21
25	13,91	0,0000	0,0026	-0,0724	-0,07
26	11,27	0,0000	0,0014	-0,0534	-0,05
27	13,20	0,0000	0,0022	-0,0667	-0,07
28	30,73	0,0000	0,1119	-0,4872	-0,50
29	16,71	0,0000	0,0050	-0,0998	-0,10
30	5,08	0,0000	0,0003	-0,0262	-0,03
31	7,20	0,0000	0,0006	-0,0334	-0,03
32	9,49	0,0000	0,0009	-0,0435	-0,04
33	11,10	0,0000	0,0014	-0,0524	-0,05
34	17,00	0,0000	0,0053	-0,1032	-0,10
35	5,29	0,0000	0,0004	-0,0268	-0,03
36	12,57	0,0000	0,0019	-0,0620	-0,06
37	13,94	0,0000	0,0026	-0,0726	-0,07
38	7,19	0,0000	0,0006	-0,0334	-0,03
39	18,99	0,0000	0,0084	-0,1297	-0,13
40	33,65	0,0000	0,1980	-0,6642	-0,68
41	12,20	0,0000	0,0018	-0,0595	-0,06
42	10,33	0,0000	0,0011	-0,0480	-0,05
43	13,56	0,0000	0,0024	-0,0695	-0,07
44	26,30	0,0000	0,0435	-0,2982	-0,30
45	27,18	0,0000	0,0527	-0,3291	-0,34
46	12,85	0,0000	0,0021	-0,0641	-0,06
47	16,49	0,0000	0,0047	-0,0974	-0,10
48	8,07	0,0000	0,0007	-0,0370	-0,04
49	8,56	0,0000	0,0008	-0,0391	-0,04
50	2,45	0,0000	0,0002	-0,0194	-0,02

TABLE 8. *(Continued.)* **Fits and diagnostics for all observations.**

51	37,50	0,0000	0,3746	-0,9688	-1,00
52	29,25	0,0000	0,0823	-0,4144	-0,42
53	6,92	0,0000	0,0005	-0,0324	-0,03
54	4,05	0,0000	0,0003	-0,0233	-0,02
55	3,99	0,0000	0,0003	-0,0231	-0,02
56	3,83	0,0000	0,0003	-0,0227	-0,02
57	4,03	0,0000	0,0003	-0,0232	-0,02
58	7,15	0,0000	0,0006	-0,0333	-0,03
59	6,20	0,0000	0,0004	-0,0298	-0,03
60	6,88	0,0000	0,0005	-0,0322	-0,03
61	5,45	0,0000	0,0004	-0,0273	-0,03
62	14,77	0,0000	0,0032	-0,0799	-0,08
63	8,94	0,0000	0,0008	-0,0409	-0,04
64	9,88	0,0000	0,0010	-0,0455	-0,05
65	14,98	0,0000	0,0033	-0,0818	-0,08
66	40,27	0,0000	0,5312	-1,2309	-1,29
67	12,73	0,0000	0,0020	-0,0632	-0,06
68	30,76	0,0000	0,1126	-0,4888	-0,50
69	15,30	0,0000	0,0036	-0,0849	-0,09
70	32,80	0,0000	0,1687	-0,6079	-0,63
71	30,08	0,0000	0,0979	-0,4539	-0,47
72	7,78	0,0000	0,0006	-0,0358	-0,04
73	5,41	0,0000	0,0004	-0,0272	-0,03
74	5,76	0,0000	0,0004	-0,0283	-0,03
75	5,92	0,0000	0,0004	-0,0289	-0,03
76	5,36	0,0000	0,0004	-0,0271	-0,03
77	8,93	0,0000	0,0008	-0,0408	-0,04
78	47,52	0,0000	0,8574	-1,9738	-2,07
79	23,60	0,0000	0,0238	-0,2196	-0,22
80	8,75	0,0000	0,0008	-0,0400	-0,04
81	9,14	0,0000	0,0009	-0,0418	-0,04
82	16,78	0,0000	0,0051	-0,1007	-0,10
83	18,91	0,0000	0,0082	-0,1285	-0,13
84	42,50	1,0000	0,6544	0,9209	0,97
85	55,51	1,0000	0,9743	0,2284	0,23
86	87,88	1,0000	1,0000	0,0055	0,01
87	37,84	1,0000	0,3931	1,3666	1,42
88	24,66	1,0000	0,0302	2,6455	2,69
89	50,03	1,0000	0,9147	0,4224	0,44
90	48,43	1,0000	0,8812	0,5030	0,53
91	47,28	1,0000	0,8505	0,5690	0,60
92	45,72	1,0000	0,7989	0,6700	0,71
93	42,68	1,0000	0,6637	0,9055	0,95
94	62,27	1,0000	0,9945	0,1054	0,11
95	41,15	1,0000	0,5812	1,0418	1,09

amount of energy generation would be lost, reconnection would require additional time, and instability of the grid would be induced. Additionally, an improvement in LVRT support could be achieved through a faster response to the fault.

It can be seen that as a result of the RTPP application, the inverter control system can achieve a time gain for moving the operating point according to the LVRT requirements and starts supporting the grid. The time gain (TG) in [s] is the difference in the timeline between the instant when the duration of the fault is estimated with the RTPP and when the sag's end is recognized with a standard algorithm (RMS). This is presented in the last column of Table 4. Based on the five voltage sags presented in Table 4, the average time gain was 1.002 s.

VII. CONCLUSION

In this paper, a novel algorithm for real-time prediction of the probability of voltage sag duration based on HF is presented. Mathematical and statistical analysis of the maximum value (MHDU) of the HF relation to the probability of sag duration is provided with adequate verification using extensive real-grid measurement data. It was shown that a voltage sag duration can be predicted (with high probability) either as ''momentary'' (if MHDU<37.7%) or as ''temporary'' (if MHDU>41.2%). In between, is the uncertain zone (37.7%<MHDU<41.2%).

The algorithm is applied to the control of grid-tie converters used in DERs and tested with real grid measurement data in the IEEE 13-bus test grid by simulations, and in the IEEE 33-bus test grid using HIL Microgrid laboratory testbed. It is shown that unnecessary tripping of wind farms and PV plants can be avoided in cases of different types of momentary sags, with benefits to residential area customers. The benefits to customers are reflected in better voltages during the faults and in avoiding unnecessary instability.

This research was based on a large set of real grid recordings and their analyses. Two different voltage levels guaranteed the diversity of the data. However, a specific S-curve that shows high reliability may differ. As this is a one-dimensional problem, it is possible to improve the reliability using neural networks to learn and adjust the probabilistic model for specific applications and under real operating conditions.

APPENDIX

Tables 6 and 7 present a detailed description of the faults obtained by measurements in a real grid, which were used in the research. Table 8 shows the fits and diagnostics for all observations.

ACKNOWLEDGMENT

The authors would like to express their acknowledgment to Prof. Math Bollen who has provided in-field measurement results, which enable formulation and verification of the proposed algorithm.

Also, their acknowledgment to the Typhoon-HIL Company, Novi Sad, Serbia, which provides the Microgrid HIL testbed for laboratory testing of the proposed method.

REFERENCES

[1] W. Dolega, "The role of distribution system operator in the context of energy security—The case of Poland," *Electr. Rev.*, vol. 87, no. 2, pp. 57–60, 2011.

[2] L. Conrad, K. Little, and C. Grigg, "Predicting and preventing problems associated with remote fault-clearing voltage dips," *IEEE Trans. Ind. Appl.*, vol. 27, no. 1, pp. 167–172, Jan./Feb. 1991.

[3] M. H. J. Bollen, *Understanding Power Quality Problems*. Hoboken, NJ, USA: Wiley, 1999.

[4] *IEEE Recommended Practice for Monitoring Electric Power Quality*, IEEE Standard 1159-2009, IEEE Standard Press, 2009.

[5] *Electromagnetic Compatibility (EMC), Part 2: Environment, Section 1: Description of the Environment, Electromagnetic Environment for Low-Frequency Conducted Disturbances and Signaling in Public Power Supply Systems*, IEC Standard 61000-2-1, IEC, Geneva, Switzerland, 1990.

[6] D. D. Sabin and A. Sundaram, "Quality enhances reliability," *IEEE Spectr.*, vol. 33, no. 2, pp. 34–41, Feb. 1996.

[7] S. C. Vegunta and J. V. Milanović, "Estimation of cost of downtime of industrial process due to voltage sags," *IEEE Trans. Power Del.*, vol. 26, no. 2, pp. 576–587, Apr. 2011.

[8] P. M. Stephens, *Power Quality Standards*, Standard IEC 61000-4-411/34, CBEMA, ITIC, SEMI FE47, 2009, pp. 2–7.

[9] V. A. Katić, "Networking harmonic pollution-review and discussion international and national standards and recommendations," in *Proc. 3rd Int. Power Electr. Cong.-CIEP*, Puebla, Mexico, Aug. 1994, pp. 145–151.

[10] M. S. Racine, J. D. Parham, and M. H. Rashid, "An overview of uninterruptible power supplies," in *Proc. 37th Annu. North Amer. Power Symp.*, Ames, IA, USA, no. 850, Oct. 2005, pp. 159–164.

[11] M. F. Mcgranaghan, D. R. Mueller, and M. J. Samotyj, "Voltage sags in industrial systems," *IEEE Trans. Ind. Appl.*, vol. 29, no. 2, pp. 397–403, Mar. 1993.

[12] T. Jauch, A. Kara, M. Rahmani, and D. Westermann, "Power quality ensured by dynamic voltage correction," *ABB Rev.*, vol. 4, pp. 25–36, Apr. 1998.

[13] H. Fujita and H. Akagi, "The unified power quality conditioner: The integration of series- and shunt-active filters," *IEEE Trans. Power Electron.*, vol. 13, no. 2, pp. 315–322, Mar. 1998.

[14] D. Graovac, V. Katić, and A. Rufer, "Power quality compensation using universal power quality conditioning system," *IEEE Power Eng. Rev.*, vol. 20, no. 12, pp. 58–60, Dec. 2000.

[15] G. Ledwich and A. Ghosh, "A flexible DSTATCOM operating in voltage or current control mode," *IET Proc.-Gener., Transmiss. Distrib.*, vol. 149, no. 2, pp. 215–224, Mar. 2002.

[16] M. Farhadi-Kangarlu, E. Babaei, and F. Blaabjerg, "A comprehensive review of dynamic voltage restorers," *Int. J. Electr. Power Energy Syst.*, vol. 92, pp. 136–155, Nov. 2017.

[17] V. Khadkikar, "Enhancing electric power quality using UPQC: A comprehensive overview," *IEEE Trans. Power Electron.*, vol. 27, no. 5, pp. 2284–2297, May 2012.

[18] M. Jalali, K. Zare, and H. Seyedi, "Strategic decision-making of distribution network operator with multi-microgrids considering demand response program," *Energy*, vol. 141, pp. 1059–1071, Dec. 2017.

[19] C. J. Wallnerström, P. Hilber, and S. Stenberg, "Fault management at a distribution system operator," in *Proc. IEEE 12th Int. Conf. Probabilistic Methods Appl. Power Syst. (PMAPS)*, Istanbul, Turkey, Jun. 2012, pp. 350–355.

[20] K. Ma, *Power Electronics for the Next Generation Wind Turbine System*, vol. 5. Cham, Switzerland: Springer, 2015.

[21] S. Kouro, M. Malinowski, K. Gopakumar, J. Pou, L. G. Franquelo, B. Wu, J. Rodriguez, M. A. Pérez, and J. I. Leon, "Recent advances and industrial applications of multilevel converters," *IEEE Trans. Ind. Electron.*, vol. 57, no. 8, pp. 2553–2580, Aug. 2010.

[22] R. Hiremath and T. Moger, "Comprehensive review on low voltage ride-through capability of wind turbine generators," *Int. Trans. Electr. Energy Syst.*, vol. 30, no. 10, pp. 1–39, Oct. 2020.

[23] *Standard for Interconnection and Interoperability of Distributed Energy Resources With Associated Electric Power Systems Interfaces*, IEEE Standard 1547-2018, IEEE Press, 2018.

[24] Y. Yang, F. Blaabjerg, and Z. Zou, "Benchmarking of grid fault modes in single-phase grid-connected photovoltaic systems," *IEEE Trans. Ind. Appl.*, vol. 49, no. 5, pp. 2167–2176, Sep. 2013.

[25] E. Afshari, G. R. Moradi, R. Rahimi, B. Farhangi, Y. Yang, F. Blaabjerg, and S. Farhangi, "Control strategy for three-phase grid-connected PV inverters enabling current limitation under unbalanced faults," *IEEE Trans. Ind. Electron.*, vol. 64, no. 11, pp. 8908–8918, Nov. 2017.

[26] A. Camacho, M. Castilla, J. Miret, L. G. de Vicuna, and G. L. M. Andres, "Control strategy for distribution generation inverters to maximize the voltage support in the lowest phase during voltage sags," *IEEE Trans. Ind. Electron.*, vol. 65, no. 3, pp. 2346–2355, Mar. 2018.

[27] R. Meyer, A. Zlotnik, and A. Mertens, "Fault ride-through control of medium-voltage converters with LCL filter in distributed generation systems," *IEEE Trans. Ind. Appl.*, vol. 50, no. 5, pp. 3448–3456, Sep./Oct. 2014.

[28] *Guide for Voltage Sag Indices*, IEEE Standard 1564, IEEE Press, 2014.

[29] I. Grcić, H. Pandžić, and D. Novosel, "Fault detection in DC microgrids using short-time Fourier transform," *Energies*, vol. 14, no. 2, p. 277, Jan. 2021.

[30] M. Farhadi and O. A. Mohammed, "Event-based protection scheme for a multiterminal hybrid DC power system," *IEEE Trans. Smart Grid*, vol. 6, no. 4, pp. 1658–1669, Jul. 2015.

[31] T. Jayasree, D. Devaraj, and R. Sukanesh, "Power quality disturbance classification using S-transform and radial basis network," *Appl. Artif. Intell.*, vol. 23, no. 7, pp. 680–693, Jul. 2009.

[32] S. Mishra, C. N. Bhende, and B. K. Panigrahi, "Detection and classification of power quality disturbances using S-transform and probabilistic neural network," *IEEE Trans. Power Delivery*, vol. 23, no. 1, pp. 280–287, Jan. 2008.

[33] A. Stanisavljević, V. A. Katić, B. Dumnić, and B. Popadić, "A comprehensive overview of digital signal processing methods for voltage disturbance detection and analysis in modern distribution grids with distributed generation," *Acta Polytechnica Hungarica*, vol. 16, no. 5, pp. 125–149, Jun. 2019.

[34] F. B. Costa and J. Driesen, "Assessment of voltage sag indices based on scaling and wavelet coefficient energy analysis," *IEEE Trans. Power Del.*, vol. 28, no. 1, pp. 336–346, Jan. 2013.

[35] V. Ignatova, P. Granjon, and S. Bacha, "Space vector method for voltage dips and swells analysis," *IEEE Trans. Power Del.*, vol. 24, no. 4, pp. 2054–2061, Oct. 2009.

[36] M. R. Alam, K. M. Muttaqi, and A. Bouzerdoum, "A new approach for classification and characterization of voltage dips and swells using 3-D polarization ellipse parameters," *IEEE Trans. Power Del.*, vol. 30, no. 3, pp. 1344–1353, Jun. 2015.

[37] T. García-Sánchez, E. Gómez-Lázaro, E. Muljadi, M. Kessler, and A. Molina-García, "Approach to fitting parameters and clustering for characterising measured voltage dips based on two-dimensional polarisation ellipses," *IET Renew. Power Gener.*, vol. 11, no. 10, pp. 1335–1343, Aug. 2017.

[38] M. H. J. Bollen and I. Y. H. Gu, *Signal Processing of Power Quality Disturbances* (Series on Power Engineering). New York, NY, USA: IEEE Press, 2006.

[39] R. Eslami, S. H. H. Sadeghi, and H. A. Abyaneh, "A probabilistic approach for the evaluation of fault detection schemes in microgrids," *Eng., Technol. Appl. Sci. Res.*, vol. 7, no. 5, pp. 1967–1973, Oct. 2017.

[40] V. A. Katić and A. M. Stanisavljević, "Smart detection of voltage dips using voltage harmonics footprint," *IEEE Trans. Ind. Appl.*, vol. 54, no. 5, pp. 5331–5342, Sep. 2018.

[41] R. Hooshmand and A. Enshaee, "Detection and classification of single and combined power quality disturbances using fuzzy systems oriented by particle swarm optimization algorithm," *Electr. Power Syst. Res.*, vol. 80, no. 12, pp. 1552–1561, 2010.

[42] H. Sha, F. Mei, C. Zhang, Y. Pan, and J. Zheng, "Identification method for voltage sags based on K-means-singular value decomposition and least squares support vector machine," *Energies*, vol. 12, no. 6, p. 1137, Mar. 2019.

[43] C. Li, J. Yang, Y. Xu, Y. Wu, and P. Wei, "Classification of voltage sag disturbance sources using fuzzy comprehensive evaluation method," *CIRED Open Access Proc. J.*, vol. 2017, no. 1, pp. 544–548, 2017.

[44] R. Turovic, A. Stanisavljevic, D. Dragan, and V. Katic, "Machine learning for application in distribution grids for power quality applications," in *Proc. 20th Int. Symp. Power Electron. (Ee)*, Novi Sad, Serbia, Oct. 2019, pp. 1–6.

[45] S. R. Fahim, S. K. Sarker, S. M. Muyeen, M. R. I. Sheikh, and S. K. Das, "Microgrid fault detection and classification: Machine learning based approach, comparison, and reviews," *Energies*, vol. 13, no. 13, p. 3460, Jul. 2020.

[46] E. A. Nagata, D. D. Ferreira, M. H. J. Bollen, B. H. G. Barbosa, E. G. Ribeiro, C. A. Duque, and P. F. Ribeiro, "Real-time voltage sag detection and classification for power quality diagnostics," *Measurement*, vol. 164, pp. 1–15, Nov. 2020.
[47] A. M. Stanisavljević and V. A. Katić, "Magnitude of voltage sags prediction based on the harmonic footprint for application in DG control system," *IEEE Trans. Ind. Electron.*, vol. 66, no. 11, pp. 8902–8912, Nov. 2019.
[48] Q. Yang, J. Lou, S. Liu, and A. Diao, "Characterization of voltage sags and its mitigation using custom power devices in emerging power system," *Bull. Electr. Eng. Informat.*, vol. 1, no. 2, pp. 69–88, Jun. 2012.
[49] M. H. J. Bollen, "Voltage sags: Effects, mitigation and prediction," *Power Eng. J.*, vol. 10, no. 3, pp. 129–135, Jun. 1996.
[50] M. N. Moschakis, S. Loutridis, V. Dafopoulos, A. Anastasiadis, T. Tomtsi, E. Karapidakis, and A. Tsikalakis, "Prediction of voltage sags applying the method of critical distances to meshed power networks," in *Proc. IEEE 12th Int. Conf. Probabilistic Methods Appl. Power Syst. (PMAPS)*, Istanbul, Turkey, Jun. 2012, pp. 570–575.
[51] M. T. Aung and J. V. Milanović, "Stochastic prediction of voltage sags by considering the probability of the failure of the protection system," *IEEE Trans. Power Del.*, vol. 21, no. 1, pp. 322–329, Jan. 2006.
[52] A. dos Santos and M. T. C. de Barros, "Voltage sag prediction for network planning," *Electr. Power Syst. Res.*, vol. 140, pp. 976–983, Nov. 2016.
[53] G. Olguin, M. Aedo, M. Arias, and A. Ortiz, "A Monte Carlo simulation approach to the method of fault positions for stochastic assessment of voltage dips (Sags)," in *Proc. IEEE/PES Transmiss. Distrib. Conf. Expo., Asia Pacific*, Dalian, China, Aug. 2005, pp. 1–6.
[54] M. Wämundson, "Calculating voltage dips in power systems using probability distributions of dip durations and implementation of the moving fault node method," M.S. thesis, Chalmers Univ. Technol., Gothenburg, Sweden, 2007.
[55] Z. Klaić, D. Šljivac, and Z. Baus, "Probability density functions of voltage sags measured indices," *J. Electr. Eng.*, vol. 62, no. 6, pp. 335–341, Jan. 2011.
[56] M. De Santis, L. Di Stasio, C. Noce, P. Verde, and P. Varilone, "Initial results of an extensive, long-term study of the forecasting of voltage sags," *Energies*, vol. 14, no. 5, pp. 1–26, 2021.
[57] V. A. Katić, S. L. Milićević, and A. M. Stanisavljević, "Voltage sags duration probability distribution function," in *Proc. 21st Int. Symp. Power Electron. (Ee)*, Oct. 2021, pp. 1–6.
[58] A. D. Santos, T. Rosa, and M. T. C. de Barros, "Stochastic characterization of voltage sag occurrence based on field data," *IEEE Trans. Power Del.*, vol. 34, no. 2, pp. 496–504, Apr. 2019.
[59] C. Noce, L. Di Stasio, P. Varilone, P. Verde, and M. De Santis, "On the forecast of the voltage sags: First stages of analysis on real systems," in *Proc. 55th Int. Univ. Power Eng. Conf. (UPEC)*, Turin, Italy, Sep. 2020, pp. 1–6.
[60] L. Di Stasio, P. Verde, P. Varilone, M. De Santis, and C. Noce, "Stochastic model to forecast the voltage sags in real power systems," in *Proc. AEIT Int. Annu. Conf. (AEIT)*, Milan, Italy, Oct. 2021, pp. 1–6.
[61] M. De Santis, L. Di Stasio, C. Noce, P. Verde, and P. Varilone, "Indices of intermittence to improve the forecasting of the voltage sags measured in real systems," *IEEE Trans. Power Del.*, early access, Mar. 21, 2021, doi: 10.1109/TPWRD.2021.3082280.
[62] D. Hosmer and S. Lemeshow, *Applied Logistic Regression*. Hoboken, NJ, USA: Wiley, 2000.
[63] C.-Y. J. Peng, K. L. Lee, and G. M. Ingersoll, "An introduction to logistic regression analysis and reporting," *J. Educ. Res.*, vol. 96, no. 1, pp. 3–14, Apr. 2002.
[64] M. Tranmer and M. Elliot, "Binary logistic regression," Cathie Marsh Inst. Social Res., Teach. Paper, 2008, vol. 2008, no. 20.
[65] A. Bagheri, M. H. J. Bollen, and I. Y. H. Gu, "Improved characterization of multi-stage voltage dips based on the space phasor model," *Electr. Power Syst. Res.*, vol. 154, pp. 319–328, Jan. 2018.
[66] C.-Y.-J. Peng, B. D. Manz, and J. Keck, "Modeling categorical variables by logistic regression," *Amer. J. Health Behav.*, vol. 25, no. 3, pp. 278–284, May 2001.
[67] J. S. Long, *Regression Models for Categorical and Limited Dependent Variables*. Thousand Oaks, CA, USA: Sage, 1997.
[68] P. D. Allison, *Measures of Fit for Logistic Regression*. Washington, DC, USA: SAS Global Forum, 2014.
[69] W. Hauckand and A. Donner, "Wald's test as applied to hypotheses in logit analysis," *J. Amer. Stat. Assoc.*, vol. 72, no. 360, pp. 1820–1852, Dec. 1977.
[70] D. R. Cox and E. J. Snell, *The Analysis of Binary Data*, 2nd ed. London, U.K.: Chapman & Hall, 1989.
[71] N. J. D. Nagelkerke, "A note on a general definition of the coefficient of determination," *Biometrika*, vol. 78, no. 3, pp. 691–692, 1991.
[72] T. Fawcett, "An introduction to ROC analysis," *Pattern Recognit. Lett.*, vol. 27, no. 8, pp. 861–874, Jun. 2006.
[73] R. Gagnon. (Dec. 30, 2021). *Wind Farm—DFIG Detailed Model (Hydro-Quebec)*. [Online]. Available: https://www.mathworks.com/help/physmod/sps/ug/wind-farm-dfig-detailed-model.html
[74] W. Zhao, X. Bi, W. Wang, and X. Sun, "Microgrid relay protection scheme based on harmonic footprint of short-circuit fault," *Chin. J. Electr. Eng.*, vol. 4, no. 4, pp. 64–70, Dec. 2018.
[75] D. Lagos, V. Papaspiliotopoulos, G. Korres, and N. Hatziargyriou, "Microgrid protection against internal faults: Challenges in islanded and interconnected operation," *IEEE Power Energy Mag.*, vol. 19, no. 3, pp. 20–35, May/Jun. 2021.

ALEKSANDAR M. STANISAVLJEVIĆ (Member, IEEE) was born in Belgrade, Serbia, in 1988. He received the B.Sc., M.Sc., and Ph.D. degrees in electrical engineering from the Faculty of Technical Sciences, University of Novi Sad, Serbia, in 2011, 2012, and 2019, respectively. He has authored/coauthored more than 30 scientific papers in international journals and conferences proceedings. His main research interests include grid integration of renewable energy, power quality, and fault detection.

VLADIMIR A. KATIĆ (Senior Member, IEEE) received the B.Sc. degree in electrical engineering from the University of Novi Sad, Serbia, in 1978, and the M.Sc. and Ph.D. degrees in electrical engineering from the University of Belgrade, Serbia, in 1981 and 1991, respectively. Since 1978, he has been with the Faculty of Technical Sciences, University of Novi Sad, where he is currently a Professor. He has participated or was the main researcher in 54 national and international research and development projects. He is the author or coauthor of many textbooks and a scientific monograph. He has also published more than 550 scientific papers in international and national journals and conferences proceedings. His research interests include power electronics converters, power quality, renewable energy sources, and electric vehicles.

SRĐAN LJ. MILIĆEVIĆ was born in 1988. He received the bachelor's degree in financial mathematics and the master's degree in applied mathematics from the Faculty of Sciences, University of Novi Sad, in 2011 and 2012, respectively, and the Ph.D. degree in mathematics in engineering from the Faculty of Technical Sciences, University of Novi Sad, in 2020. His research interest includes numerical linear algebra and its applications.